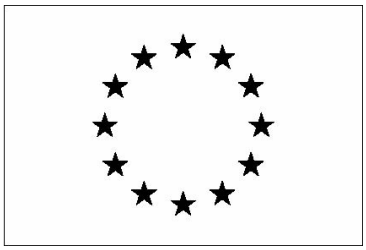

Grant Agreement number: **248095**

Project acronym: **Q-ESSENCE**

Project title: **Quantum Interfaces, Sensors, and Communication based on Entanglement**

Funding Scheme: **Collaborative Project (Large-Scale Integrating Project)**

DELIVERABLE REPORT

Deliverable no.:	**D 2.3.3**
Deliverable name:	**Report on multimode light-matter interfaces**
Workpackage no.	**WP 2.3**
Lead beneficiary	**UWAW**
Nature	**R = Report**
Dissemination level	**PU = Public**
Delivery date from Annex I (proj month)	**30/04/2013**
Actual / forecast delivery date	**30/04/2013**
Status	**Submitted**

Introduction

In this deliverable we report the progress towards creating robust, multi-mode, light-matter interfaces using certain modes of quantum electromagnetic fields and atomic systems with long-lived coherence. Here we concentrate on developing mutual agreement between theoretical description and experimental results for a multimode photon generator based on a Raman interface.

Eigen-mode description of light-matter interfaces

We have reformulated the problem of Raman scattering in atomic vapours in the limit of low scattering intensity [KCW1-12]. It is then possible to find eigen-modes of the problem that are only pairwise coupled. The entire quantum light field can be decomposed in a, typically unique, basis in which distinct modes are not coupled to one another despite complicated interaction with a large cloud of three-level atoms. Likewise the atomic excitations can be cast into a convenient basis in which distinct spin-waves are not coupled by the beam inducing Raman transitions. However, each light mode has its twin atomic mode with which it is engaged in two-mode squeezing with the squeezing parameter proportional to the driving pulse intensity and duration and the eigen-value of the mode pair in question. The eigen-modes for light are close to La Guerre-Gauss Beams and similarly for the atoms however truncated to extents of the atomic sample. The total number of significantly populated eigen-modes is of the order of the Fresnel number of illuminated portion of the atomic sample.

This model allows for straightforward inclusion of the decoherence, which is incorporated into the evolution equations for each pair of coupled light-atom modes. The corrected equations are easily solved and analytical predictions regarding population of the modes and their correlations can be made. In particular we find threshold pump intensity for exponential growth of the number of scattered photons.

Experimental characterisation of multimode structure

The theoretical predictions were verified in an experiment with warm 87-Rb vapour [CW2-12]. We measured the number of photons scattered in the Stokes and subsequently anti-Stokes scattering to create spin-waves and subsequently convert them back to light. This way we could probe the exponential growth of the scattering and the decoherence of the spin-waves in the dark. We collected scattered light on a camera in the far field to probe many scattering angles, and thus many K-vectors, concurrently. The results of the measurements agree with theoretical predictions concerning the growth and the number of the populated modes.

We have also estimated the number of stored modes as a function of storage time and found it to quickly decay to 1. However we also identified the primary reason for this behaviour to be diffusion in the buffer gas.

Experimental investigations of decoherence

Following the findings of the previous experiments we proceeded with precise characterisation of the decoherence at the storage state in our multimode atomic memory. We identified that it almost exclusively due to diffusion and thus we decided to measure the diffusion rate precisely for various buffer gases and pressures. With the Raman scattering at hand we were able to develop completely new method of measuring diffusion, which is well suited to modern applications [CW1-13]. We believe it is a true breakthrough compared to methods developed by Franzen 50 years ago and still in use.

We were the first to try Xenon as a buffer gas and we made the first ever measurements of diffusion of Rubidium in it, which strongly suggests it is the best buffer gas for spatially multimode quantum memories.

Time-bin encoding multimode atomic memory

The Raman atomic memory can be also used to coherently store a light pulse and multiplex it between subsequent temporal modes [RNJ1-12]. The approach pursued at UOXF:DU uses 300ps laser pulses to achieve over GHz bandwidth without loss of available storage time. Their work demonstrates possibility of splitting the information stored in a single spin-wave mode among many temporal modes of light. For instance, storage of a single photon, followed by partial retrieval using three read pulses creates a time-bin entangled W-state. In addition they have also verified the memory, that is the process of storage and retrieval, is coherent. This is demonstrated in an experiment in which output signals from two independent memories interfere.

Conclusions

We reported a number of steps towards creating robust, multi-mode light-matter interfaces between certain modes of quantum electromagnetic fields and atomic systems with long-lived coherence. These included developing simple multimode theoretical model and test its predictions against experimental results as well as devising ways to circumvent decoherence and pursuing time-bin multimode atom-light interfaces.

References:

[KCW1-12] J. Kolodynski, J. Chwedenczuk and W. Wasilewski, *Eigenmode description of Raman scattering in atomic vapors in the presence of decoherence*, Phys. Rev. A 86 013818 (2012)

[CW2-12] R. Chrapkiewicz and W. Wasilewski, *Generation and delayed retrieval of spatially multimode Raman scattering in warm rubidium vapors*, Opt. Express 20 29540 (2012)

[CW1-13] R. Chrapkiewicz, W. Wasilewski and C. Radzewicz, *How to measure diffusional decoherence in multimode Rubidum vapor memories?* (2013) arXiv:1304.5396

[RNJ1-12] K. F. Reim, J. Nunn, X-M. Jin, P. S. Michelberger, T. F. M. Champion, D. G. England, K. C. Lee, W. S. Kolthammer, N. K. Langford, I. A. Walmsley, *Multipulse Addressing of a Raman Quantum Memory: Configurable Beam Splitting and Efficient Readout*, Phys. Rev. Lett. 108 263602 (2012)

How to measure diffusional decoherence in multimode Rubidum vapor memories?

Radosław Chrapkiewicz,* Wojciech Wasilewski, and Czesław Radzewicz
Insitute of Experimental Physics, University of Warsaw, ul. Hoża 69, 00-681, Warsaw, Poland
(Dated: April 22, 2013)

Diffusion is the main limitation of storage time in multispatial mode applications of warm atomic vapors. Surprisingly, there is scarce data for diffusion coefficients of Rubidium in buffer gases and available measurement methods are poorly suited to modern experiments. Here we present a simple, efficient and direct method of measuring diffusion coefficients in gases by creating, storing and retrieving spatially-varying atomic coherence. Raman scattering provides a necessary interface to the atoms that allows for probing many spatial periodicities concurrently. We single out the diffusional component of depolarization and determine the diffusion coefficient.We found the normalized diffusion coefficients for Rubidium atoms in noble gases to be as follows: Neon 0.20 cm^2/s, Krypton 0.068 cm^2/s, Xenon 0.057 cm^2/s. We are the first to give experimental results for Xenon and we recommend this gas for multimode quantum storage applications.

PACS numbers: 51.20.+d, 42.50.Hz, 42.50.Gy, 42.65.Dr

I. INTRODUCTION

In recent years warm atomic ensembles have been widely used in many applications in quantum optics and atomic physics. The most promising applications include quantum repeaters [1], quantum memories [2] and ultra-precise magnetometry [3]. They have also been shown to be an effective medium for four-wave mixing processes [4], Electromagnetically Induced Transparency (EIT) [5] and slow light generation [6].

An advantage of using warm atomic gas is undoubtedly the simplicity of performing the experiment and obtaining large optical depths. However, it entails fast thermal motion of atoms. Atomic motion limits the efficiency of many modern systems that use multimode properties of atomic ensembles. At best this motion can be slowed down and made diffusive by addition of a suitable buffer gas. Thus, it is important to know the diffusion coefficients for proper experiment design and interpretation.

An important example of systems limited by diffusion is storing and retrieving transverse modes and images in Gradient Echo Memory (GEM) [7, 8], in collective Raman scattering [9] or in Electromagnetically Induced Transparency (EIT) [10]. Typically diffusional motion of atoms in a buffer gas limits the storage time of images down to tens of microseconds [11, 12] or restricts the number of spatial modes retrieved [9]. In other experiments based on EIT diffusion broadens the EIT spectrum [13]. Knowledge of the exact diffusion coefficient is required to design diffraction cancellation [14].

Based on the aforementioned examples we envisage that using multimode properties of atomic ensembles will become increasingly important in the nearest future. Given this fact, one of the most important defies will be to master diffusion processes so as to go beyond current limitations. Reading through the papers we found all of them to have two features in common. In none of them the choice of the buffer gas type and pressure was well-founded, nor was the diffusion coefficient reliably measured. There has been no attempt to optimize experimental conditions by controlling diffusion coefficients and knowledge of the value of the coefficient itself was rather doubtful.

Most of the experiments with EIT and GEM listed above used Rubidium embedded in Neon buffer gas. This was probably due to the favorable ratio of diffusion coefficient to spin depolarization cross section in this gas which made it standard in optical pumping and magnetometry experiments. The values of diffusion coefficient of Rubidium atoms in Neon referenced up to date were measured 50 years ago with substantial effort and care [15, 16]. However, probably due to indirectness of methods available those days, the diffusion values obtained in [15, 16] differ by more than 50%. Diffusion measurements for Neon had been conducted several times before the 1970s alongside measurements of spin relaxation cross sections [15–18]. The values given in these papers differ from each other up to 3 times.

To our knowledge only one Australian group tried to use Krypton in the context of quantum memories in their GEM experiment [19]. This is a sensible choice when it comes to fighting diffusion, since it is almost 3 times slower in Krypton than in Neon at the same pressure. However, the Australian group does not quote any experimental measurements of diffusion. In their most recent paper [8] the authors measured the value of the diffusion coefficient using updated method of Franzen [20, 21]. They compared this measurement with the values they had inferred from the lifetime of the memory and with theoretical calculations, getting up to 500% differences. We take it as a motivation to perform measurements using up to date method, all the more since we have been able to find only one paper from 1972 that gives the diffusion coefficient for Rubidium in Krypton [22].

We have been surprised by the scarceness and limited reliability of data on the diffusion of Rubidium in no-

* radekch@fuw.edu.pl

ble buffer gases. We have seen a considerable need for reliable results which, we believe, will help design novel experiments with the multimode use of atomic ensembles. Therefore we have decided to present a method for measuring diffusion coefficients that is easy to implement, robust and up to date. We also believe that gases different from those that have been used so far can turn out to be even more effective.

Given the latest applications of hyperpolarized Xenon, it would be useful to have reliable data on the diffusion of Rubidium in that gas as well [23]. Yet, it turns out that its diffusion coefficient has never been measured but it was only deduced from cross sections of velocity changing collisions. We have measured and list herein the values of the diffusion coefficients for Neon, which is the most popular, and Krypton we are the very first to give the value of this coefficient for Rubidium diffusion in Xenon.

This paper is organized as follows. In Sec. II we summarize previous methods for measuring diffusion coefficients based on examining spin relaxation and spot out their weaknesses. In Sec. III we introduce the principles of our method. Sec. IV describes in detail the experimental implementation. Sec. V contains the experimental results. Finally, Sec. VI concludes the paper.

II. METHODS OF MEASURING DIFFUSION COEFFICIENTS

A. Previous methods

We can affirm that problems with considerable uncertainty and scarceness of data for diffusion coefficients of alkali atoms in buffer gases result from complexity of the measurement methods themselves. There were designed primarily for the purpose of measuring the cross section of spin-exchange collisions.

The pioneering method that involved measuring diffusion coefficients was proposed by Franzen in 1959 [15], and all of the subsequent contributions used the initial conception unchanged or slightly improved. Franzen measured longitudinal relaxation time of pumped Rubidium atoms in Neon or Argon buffer gas. He applied a pump probe method through which he examined the change in absorption of the probe beam as a function of depolarization time and buffer gas pressure. In order to retrieve the diffusion coefficient from such measurements, Franzen made a few assumptions. He theorized that atoms depolarize owing to Rb-Rb collisions, Rb-buffer gas collisions, and fully depolarize in contact with walls. He also assumed the cell was a uniformly illuminated cylinder. Consequently, he obtained the formula for average atom relaxation time as a function of buffer gas pressures. In the vacuum the relaxation was due to the atomic motion, while at high gas pressures it was mainly due to spin exchange collisions. Thus, by fitting dependence of the relaxation time on pressure with theoretical formula, Franzen and his followers were able to find spin depolarization cross section and diffusion coefficient. This procedure requires precise knowledge of temperature, Rb-Rb depolarization cross section, pressure and cell dimensions. The assumptions made at the beginning are virtually impossible to verify. Nevertheless, [15] had a profound significance for the future research dealing with diffusion of Rubidium atoms, since among many it presents both decent experimental results and sensible conjectures.

Franzen's method [15], without further alterations, was used to measure diffusion coefficient in various buffer gases and conditions [16, 24, 25]. The method was modified later to measure not only longitudinal, but also transversal decay of polarization [17, 18]. A certain innovation introduced afterwards was the use of a spatially limited beam [20] and thereafter a laser beam [21] to probe polarization distribution in the cell volume by changing the position of the probe beam.

By applying the Franzen's method one cannot measure the diffusion coefficient for gases with a large spin depolarization cross section. This is why the diffusion coefficient for Krypton was measured only once [22] and there is no experimental data on the diffusion coefficient for Rubidium in Xenon.

All of the papers mentioned above were based on the probing of spin relaxation evolution in the whole cell. They varied pulse duration, beam separation, pressure and the resulting diffusion coefficient was usually one of many fit parameters. Their results display large spread with discrepancies up to 300%.

Recent attempts to calculate the diffusion coefficient from updated Franzen's method [20, 21] and GEM storage times also exhibit an appreciable spread [8]. Nevertheless the Franzen and his followers are still cited and, as far as we know, there have been no measurements using significantly different techniques.

B. Description of the new method

Diffusion of alkali metals in buffer gases imposes a significant limitation on storage time in contemporary experiments with atomic ensembles. Attempts to repeat complex methods of Franzen and followers mentioned afore were not effective while no alternative methods have been presented. Thence, we propose a new, up-to-date and simple method for measuring diffusion coefficients.

In our method we probe depolarization of fast spatially changing atomic coherence. Atomic coherence is blurred over time by diffusion as shown in Fig. 1. Thus, we expect high spatial periodicity components of the coherence to disappear faster than those varying slowly. By measuring decay rates for patterns of different periodicities we are able to retrieve the diffusion coefficient. Spatial periods of created atomic coherence patterns are much smaller than the cell size, therefore the influence of the walls can be neglected altogether.

Patterns of atomic coherence are created through spon-

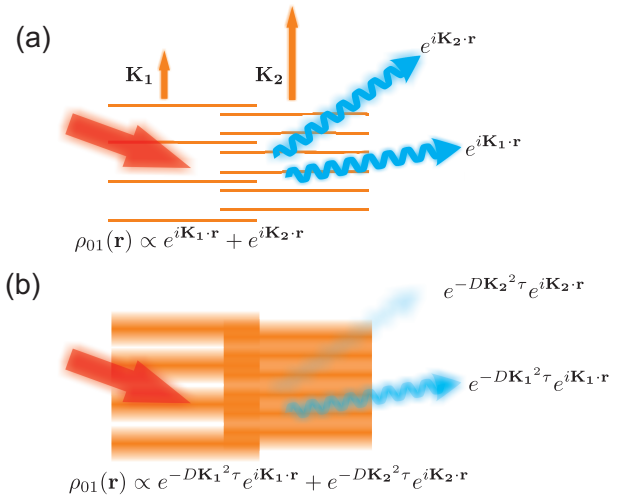

Figure 1. (Color online) (a) Planewave components of spatially dependent atomic coherence $\rho_{01}(\mathbf{r})$ act as diffraction gratings deflecting laser beam at different angles. (b) Components of high periodicity are blurred faster due to diffusion, therefore intensity of deflected light will decay faster for higher angle of deflection. During storage time τ, pattern component of specific periodicity corresponding to wave vector $\mathbf{K}$ blurs with decay rate $D\mathbf{K}^2$, where D is the diffusion coefficient.

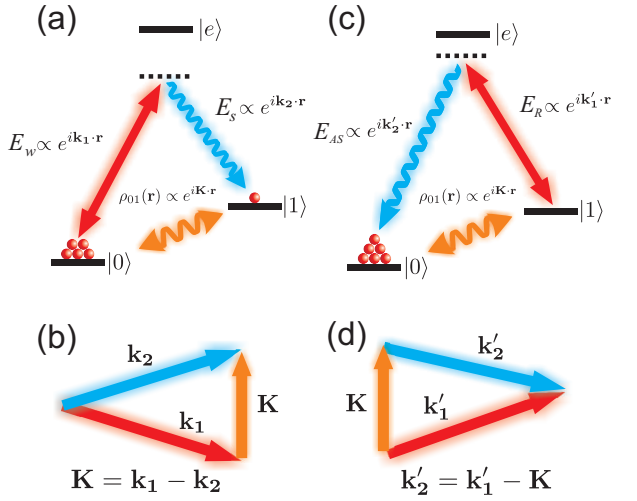

Figure 2. (Color online) (a) Atomic coherence $\rho_{01}(\mathbf{r})$ is created in spontaneous Stokes scattering. (b) Difference between wave vectors of laser field $\mathbf{k_1}$ and scattering field component $\mathbf{k_2}$ is stored in the spatially dependent phase of the atomic coherence. (c) Atomic coherence can be converted back to light in anti-Stokes scattering. (d) Atomic coherence phase is imprinted on anti-Stokes scattering as momentum conservation. Unlike the Stokes process, anti-Stokes scattering deterministically retrieves created coherence pattern on demand.

taneous (Stokes) Raman scattering. Each pattern comprises many plane-wave components with different periodicities. Those components decay at a different rates due to diffusional motion of the atoms. After a certain storage time a relative contribution of each plane-wave component to the pattern can be measured by driving anti-Stokes scattering. Then each plane-wave component acts as a diffraction grating deflecting driving laser beam as illustrated in Fig. 1 (a). By measuring the intensity of the Stokes scattering light as a function of deflection angle and time between pattern creation and readout, we can calculate the lifetime of different plane-wave components constituting atomic coherence. This represents a sizable amount of data containing information about homogeneous decay rate and the diffusion coefficient. Values of those coefficients are easily retrieved through observing that only diffusion gives rise to an excess in periodicity-dependent decay rate. Below we develop formulas describing the process.

III. THEORY

A. Diffusion of atomic coherence field

Our method relies on creating, storing and probing spatially dependent coherence $\rho_{01}(\mathbf{r})$ between two long lived atomic levels $|0\rangle$ and $|1\rangle$. We observe the diffusion at the storage stage. As atoms move, coherence in a specific point $\mathbf{r}_0$ will reshuffle its values with the neighboring points. Evolution of atomic coherence in the dark will be described by the equation of diffusion with coefficient D and homogeneous depolarization with rate γ_0 [7, 26]:

$$\frac{\partial}{\partial t}\rho_{01}(\mathbf{r},t) = D\nabla^2\rho_{01}(\mathbf{r},t) - \gamma_0\rho_{01}(\mathbf{r},t) \qquad (1)$$

Evolution of each plane wave component of initial amplitude $\beta(K)$ and wave vector K is described by a simple exponential decay at a rate $\gamma(\mathbf{K}) = \gamma_0 + DK^2$.

In general, the spatially dependent coherence $\rho_{01}(\mathbf{r})$ is a superposition of many plane waves of initial amplitudes $\beta(K)$, each decaying at a specific rate:

$$\rho_{01}(\mathbf{r},t) = e^{-\gamma_0 t}\sum_{\mathbf{K}}\beta(K)e^{-DK^2t}e^{i\mathbf{K}\cdot\mathbf{r}} \qquad (2)$$

By measuring decay rates $\gamma(K)$ as a function of wave vector K we can infer diffusional depolarization DK^2 because it is the only contribution to the decay rate $\gamma(K)$ depending quadratically on K.

B. Creation and probing of atomic coherence: Raman scattering

The spatially dependent coherence $\rho_{01}(\mathbf{r})$ between ground levels of Rubidium can be both created and probed by inducing Raman scattering.

In Fig. 2(a) we illustrated the atomic levels involved in the Stokes scattering leading to creation of coherence $\rho_{01}(\mathbf{r})$ between levels $|0\rangle$ and $|1\rangle$. Upon spontaneous scattering of laser beam detuned from the $|0\rangle \leftrightarrow |e\rangle$

transition both the scattered light and atomic coherence are created. We shall consider a simple case where the laser beam and the scattered light are planewaves with the wave vectors, $\mathbf{k_1}$ and $\mathbf{k_2}$, respectively. The difference between the laser field wave vector $\mathbf{k_1}$ and the created photons wave vector $\mathbf{k_2}$ is accumulated in atoms as a spatial phase of atomic coherence. As illustrated in Fig. 2(b) the atomic coherence created will be of a form $\rho_{01}(\mathbf{r}) = \beta e^{i\mathbf{K}\cdot\mathbf{r}}$, where $\mathbf{K} = \mathbf{k_1} - \mathbf{k_2}$.

Such periodic atomic coherence $\rho_{01}(\mathbf{r})$ can work as a diffraction grating and deflect a laser beam. This is realized in the anti-Stokes scattering process presented in Fig. 2(c) in which laser beam detuned from the $|1\rangle \leftrightarrow |e\rangle$ transition is scattered at an angle. The spatial phase of atomic coherence $\rho_{01}(\mathbf{r})$ is imprinted back onto scattered photons as follows from Bragg condition. Provided driving laser beam is the plane wave with a wave vector $\mathbf{k_1'}$ the diffracted light wave vector will be $\mathbf{k_2'} = \mathbf{k_1'} - \mathbf{K}$ as illustrated in Fig. 2(d). Therefore by observing the intensity of the light $I_{AS}(\theta)$ scattered at an angle θ, we register a signal which is proportional to the modulus square of the corresponding plane wave component of atomic coherence $|\beta(K)\exp(-\gamma(K)t)|^2$, with $\theta = K/k_1' = K\lambda/2\pi$.

C. Averaging and retrieving diffusion coefficient

We create spatially varying atomic coherence $\rho_{01}(\mathbf{r})$ in the spontaneous Stokes scattering process, which populates various planewave components randomly. Nonetheless, the average modulus square of the excitation amplitude $\langle|\beta(K)|^2\rangle$ created right after the scattering is set by the driving pulse parameters and can be kept constant between measurement series. Therefore, we can calculate average intensity of the light scattered at a certain angle $\theta = K/k_1'$ and for the given storage time τ, incorporating Eq. (2):

$$\langle I_{AS}(\theta = K/k_1', \tau)\rangle = \eta(K)\langle|\beta(K)|^2\rangle e^{-2\gamma(K)\tau} \qquad (3)$$

where $\eta(K)$ is an efficiency of readout, *a priori* dependent on K. The only factor that depends on the diffusion time τ is the intensity decay factor $e^{-2\gamma(K)\tau}$, which provides direct information about the decay rate $\gamma(K)$. Therefore for a given angle of observation $\theta = K/k_1'$ we can infer $\gamma(K)$ from an exponential fit to a series of experimental data taken for successive τ.

By repeating the decay fits for many K we can gather and then fit the expected functional dependence $\gamma(K) = \gamma_0 + DK^2$, to obtain the diffusional coefficient D. In principle, we could use only two measurements of decay rates γ corresponding to just two different directions. Note that thanks to particular way of populating the spatially varying atomic coherence, we create and probe many wave vectors concurrently without altering the setup. Thence we obtain many points corresponding to a broad span of K vectors in a single measurement sequence, which provides for a robust quadratic fit of $\gamma(K)$. The quality and reliability of the experimental data is directly reflected in this last fit.

D. Angular blurring at readout

So far we have assumed the driving beam to be a planewave. The finite size w of the driving laser beam in anti-Stokes scattering results in limited resolution in probing a wave vector space. The angular spread of the laser beam driving the readout will be transferred onto the angular distribution of the scattered light due to the momentum conservation even for a planewave atomic coherence $\rho_{01}(\mathbf{r})$. Thus for any specific angle of observation $\theta = K/k_1'$ we detect scattered light originating from several distinct Fourier components of atomic coherence pattern. The contribution will come from the component of the wave vector K and its vicinity to the spread σ. We expect the spread σ to be of the order of the inverse of the driving laser beam size $1/w$.

The result of the limited resolution is an overall increase of the observed decay rates γ_{obs}. It can be estimated by convolving the storage time-dependent Fourier distribution of atomic coherence $\rho_{01}(\mathbf{r})$ with a Gaussian of a spread σ, yielding:

$$\gamma_{obs}(K) = (\gamma_0 + 2D\sigma^2) + DK^2 \qquad (4)$$

Note that the term quadratic in K in the above formula did not change, therefore the procedure to obtain the diffusion coefficient D remains unchanged. We only have to assure that the term $2D\sigma^2$ is small compared to DK^2. This can be done by increasing the beam size w.

In conclusion all measurements can be completed by varying only the one parameter – the diffusion time τ equal to laser pulse separation while collecting scattered light on the camera. Data analysis require three straightforward steps: averaging, exponential and eventually quadratic fit to obtain D. This makes the whole procedure relatively quick and simple to repeat.

IV. EXPERIMENT

In our case the levels $|0\rangle$ and $|1\rangle$ between which we create atomic coherence $\rho_{01}(r)$ are hyperfine split levels $5_2S_{1/2}$, F=1 and F=2 respectively. Spatially dependent coherence $\rho_{01}(r)$ is created and read with the use of Raman transitions between this levels. The scattered light is separated from much stronger stimulating lasers by a polarizer and additionally filtered out spectrally by Rubidium 85 filtering cell. The scattered light is registered by an Electron Multiplying CCD (Hamamatsu) camera sensor which is placed in the far field. The main part of the experimental setup is shown in Fig. 3, further details can be found in [9].

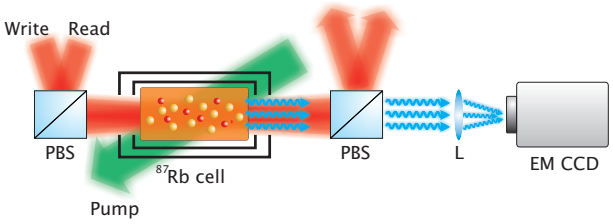

Figure 3. (Color online) Central part of the experimental setup. Rubidium-87 atoms are mixed with the buffer gas in a glass cell inside a double magnetic shielding. Pump, write and read are the laser beams used to prepare atoms in the ground state $|0\rangle$, create and probe atomic coherence patterns respectively. Stokes and anti-Stokes scattering are singled out on polarizing beam splitter PBS and observed in the far field on the electron multiplying EM CCD camera.

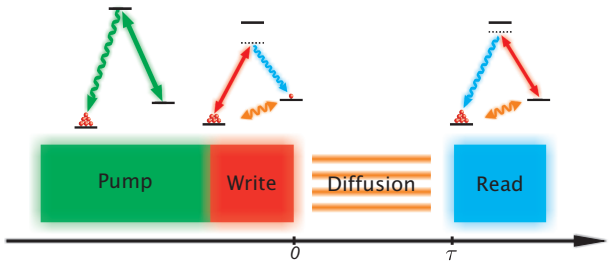

Figure 4. (Color online) Single operational sequence. First Rubidium atoms are pumped on D2 line to F=1 ground level $|0\rangle$. Then spontaneous Stokes scattering is driven to create spatially varying atomic coherence. Next we store the coherence in the dark for time τ and we let it fade due to diffusion. Finally we probe the coherence driving anti-Stokes scattering .

The operational sequence is shown in Fig. 4. Laser pulses were formed with the use of acousto-optical modulators. We began with optical pumping of Rubidium atoms to the ground state F=1. The pump laser operates in resonance on D2 line. Then we created random patterns of atomic coherence in the Stokes scattering process driven by 2-5 μs pulses of the write laser detuned from the F = 1→F' = 1 D1 transition line by 1 GHz to the red. The Stokes scattering was recorded with a camera for diagnostic purposes. Next the atoms were left to diffuse for time τ. Finally we used 5 μs long pulses of read laser detuned 1 GHz from the F = 2→F' = 2 D1 transition line to the blue to probe blurred atomic coherence $\rho_{01}(\mathbf{r})$ and record anti-Stokes scattering intensity in the far field $I_{AS}(\theta)$.

Beam diameters $1/e^2$ and powers for the Stokes and anti-Stokes drive laser were 5 mm, 4 mm and 16 mW, 7 mW respectively. They were chosen in order to achieve both good resolution as discussed above Eq. (4) and a sufficient scattering rate [9].

We repeated the create-store-read sequence multiple times and recorded random patterns of anti-Stokes scattering, changing the storage time τ.

We used four Rubidium 87 cells with different buffer

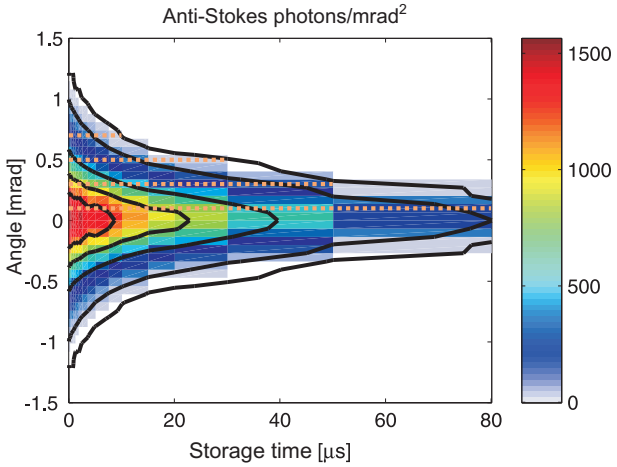

Figure 5. (Color online) Average number of photons per pixel $\langle I_{AS}(\theta,\tau)\rangle$ in anti-Stokes scattering process as a function of the storage time τ and angle of observation θ. Data taken for a cell with 1 torr Xenon. The decay is conspicuously faster for higher angles of scattering. The contour lines show 1200, 800, 400, 50, 10 photons per pixel.

gases. Those were: Neon - the most popular and the best explored, at the pressure of 2 torr, Krypton - which had been used in similar cases and we had some data concerning its diffusion coefficient, at 0.5 torr and 1 torr as in: [19] and [8] respectively. Xenon – though its diffusion coefficient had not been measured before, we presumed it to be the smallest (due to the specific weight of the gas). All cells were 10 cm long, 2.5 cm diameter cylinders made by Precision glassblowing. The longest times for anti-Stokes scattering observations were ca. τ =50 μs, which corresponded to an RMS atomic displacement of about 1 mm, far less than the cell size.

The cells temperature was stabilized at ca. 70° C, which corresponded to an optical depth of 40 and a concentration of rubidium atoms $n = 10^{12}$ cm^{-3}. Cells were heated with bifilar windings, but the heating current was interrupted for the time of impulse sequence inducing Raman scattering. The cells were placed inside a double magnetic shield.

For each diffusion time τ we averaged 500 images of anti-Stokes scattering each time obtaining smooth symmetric profiles. We subtracted the averaged background. Given that the most important thing for us is the intensity as a function of azimuth angle θ, we also carried out a polar averaging around the laser beam direction increasing signal to noise ratio. The result of the measurements was average scattering intensity $\langle I_{AS}(\theta,\tau)\rangle$ as a function of angle θ and storage time τ.

V. RESULTS

In Fig. 5 we present a typical map of the averaged angular profiles of anti-Stokes scattering in cell with Xenon

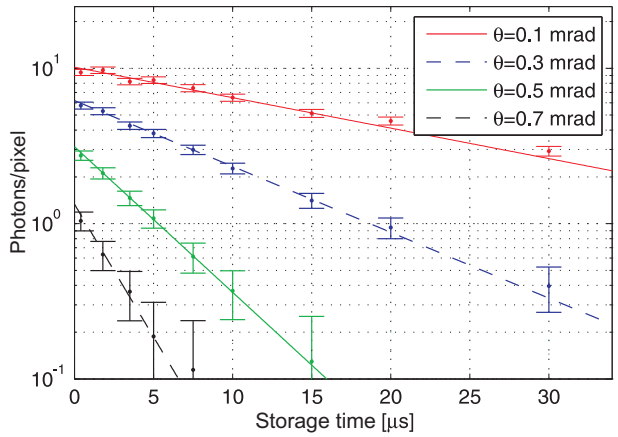

Figure 6. (Color online) Average number of photons per pixel $\langle I_{AS}(\theta,\tau)\rangle$ as a function of storage time τ with exponential decay fits observed for four different angles θ. Decays are visibly faster for higher scattering angles. Data corresponds to horizontal dashed lines in Fig. 5.

vs free depolarization time $\langle I_{AS}(\theta,\tau)\rangle$. The results are given as a function of the scattering angle θ, which is proportional to the wave vector of the corresponding Fourier components of atomic coherence patterns $\theta = K\lambda/2\pi$.

In Fig. 6 we plot an average number of photons as a function of storage time τ at a few angles θ marked with dashed lines in Fig. 5. The decay rate is faster for higher angles of scattering. The error bars in Fig.6 correspond to 1σ uncertainty and were calculated from the full statistics of camera counts. We fit exponential decays to the data taking the error bars into account. It is worth underlining that the data fits well to the curve at each scattering angle. As shown in Fig. 6, for high scattering angles θ the average signal $\langle I_{AS}(\theta,\tau)\rangle$ is at the level of one photon per shot which increases the uncertainty of γ considerably.

A. Retrieving diffusion coefficients

Having obtained an exponential fits for decays in all directions, we can analyze decays rates $\gamma_{obs}(\theta)$ as a function of the deflection angle θ. In Fig. 7(a) we present fitted decay rates for measurements in cells filled with 1 torr of Xenon as well as with 2 torr of Neon . In Fig. 7(b) we give measured data for cells with Krypton at two pressure values: 0.5 torr and 1 torr.

As expected, the data fits to the quadratic dependence $\gamma_{obs}(\theta) = \gamma_{0,obs} + D\theta^2(2\pi/\lambda)^2$. Now our 1σ error bars correspond to respective confidence bound from the exponential fit. Note that for high decay rate values the uncertainties are large because they correspond to small and noisy signals.

The measurements described above were repeated several times in order to make sure the results were reliable and repeatable. We changed the amount of the light generated by altering pulse duration of the writing laser and repeating measurements at different temperatures. The spread of diffusion coefficients obtained was about 5-12%, depending on the cell. We attribute this spread to beam wander, laser power and frequency instability and the drift of the temperature of the cell during each measurement sequence.

Buffer gas	Pressure [torr]	D[cm^2/s]	$\gamma_{0,obs}$ [kHz]
Ne	2	91 ± 11	38
Kr	0.5	136 ± 9	71
Kr	1	57.5 ± 3	28
Xe	1	52 ± 3	33

Table I. Fit parameters for measured cells. Temperature: 70° C .

In Tab. I we summarize fitted values from the measured data from charts in Fig. 7. Note, that for measurements in Krypton the ratio of obtained diffusion coefficients is close to the nominal pressure values.

To further verify the accuracy of our results, we carried out reference measurements for Krypton at 1 torr using write and read beams reduced ca. 3 times, so that their diameters $1/e^2$ were 1.6 mm i 1.4 mm respectively. This time the measurement was definitely less accurate due to the spread of wave vectors of the read beam and due to aberrations in the imaging system. The diffusion coefficient measured lay within the range of 40 cm^2/s to 65 cm^2/s, which is consistent with other results .

Finally let us note, that the observed decay rate at $K = 0$, $\gamma_{0,obs}$ summarized in Tab. I is dominated by excess contribution due to finite read beam size, $2D\sigma^2$ in Eq. (4). From respective collisional cross sections [16] we estimate ca. 1.5 kHz of decay rate due to Rb-Rb collisions and contributions less than 150 Hz from Rb – buffer gas collisions.

B. Normalized diffusion coefficients

To conclude, we shall present diffusion coefficients D_0 normalized to the standard conditions, i.e. at atmospheric pressure and at 0° C. They are related to the measured diffusion coefficients as follows:

$$D_0 = D\left(\frac{P}{760\ \text{Torr}}\right)\sqrt{\frac{T_0}{T}} \qquad (5)$$

Where P stands for gas pressure at $T_0 = 0°$C, T – temperature upon measurement. Diffusion coefficient will scale as $T^{1/2}$ according to [27]

The temperature is known with good accuracy and the main error in determining D_0 results from inaccuracy of gas pressure in cells, specified by the producer not to be worse than 10%, and from the spread of measured D values. Normalized diffusion coefficients are listed in Tab. II together with data published previously.

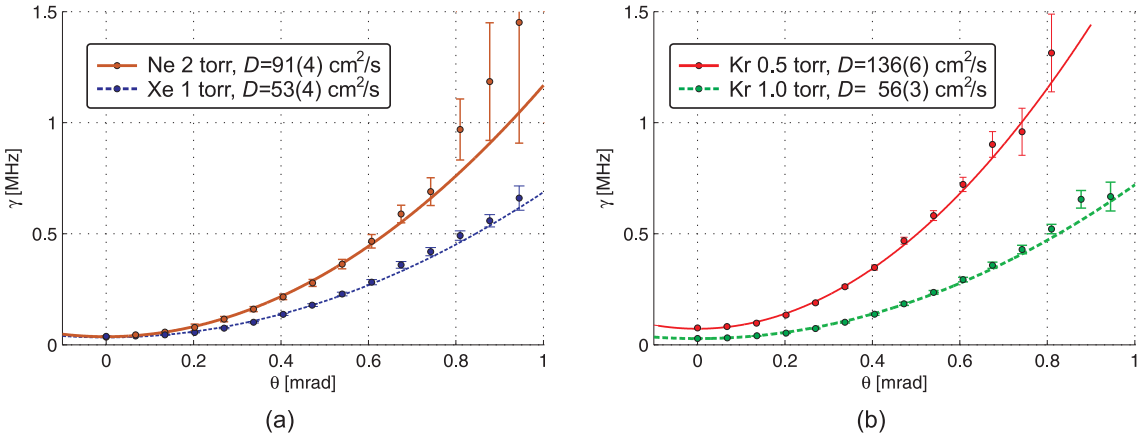

Figure 7. (Color online) Decoherence rates $\gamma(\theta)$ as a function of scattering angle corresponding to the atomic coherence wave vectors $K = 2\pi\theta/\lambda$. We fit the data with quadratic dependence $\gamma_{obs}(\theta) = \gamma_{0,obs} + D\theta^2(2\pi/\lambda)^2$. Quadratic term of fit gives diffusion coefficient D. (a) Data taken for 1 torr of Xenon and 2 torr of Neon (b) Data taken for Krypton of different pressures 0.5 torr and 1 torr.

Buffer gas	D_0[cm^2/s] – this paper	D_0[cm^2/s] - previous results
Ne	0.20±0.02	0.11 [11], 0.18 [18], 0.31 [15, 17], 0.48 [16]
Kr	0.068±0.006	0.1 [22] 0.007 [8]
Xe	0.057±0.007	No experimental data

Table II. Measured diffusion coefficients of Rubidium atoms in noble buffer gases: Ne, Kr, Xe. Results are normalized to 0°C and 760 torr pressure.

The results we obtained do not differ from those obtained beforehand, which – as we can see from Tab. II– were characterized by a noticeable spread.

VI. CONCLUSIONS

We have demonstrated a novel method for measuring diffusion coefficients of atoms in buffer gasses tailored to atomic memory applications. The method is based on creation of spatially varying atomic coherence fields, letting them diffuse in the dark and probing them. The fields comprise various spatial periodicities evolving concurrently, created and probed with Raman scattering.

A diffusion is observed in the dark and it is the only mechanism to produce periodicity dependency in the decay rate. With our approach, the evolution of the components of the atomic coherence with various periodicities can be observed in parallel and the periodicity dependency in the decay rate can be singled out easily. This leads to quite direct determination of the diffusion coefficient founded on a basic time and angle calibrations of the experimental setup. However, our method also relies on using lasers of a few MHz frequency stability and magnetic shielding.

We have verified that the method is accurate and repeatable. Results are based on multiple independent measurements for a number of various K vectors which give almost the same values. We also checked that varying laser beam widths and detunings does not affect the final result and that it scales properly with gas pressure.

We suppose that our method could be incorporated into experiments in which diffusion is the limiting factor, such as GEM, EIT, quantum memories or collective Raman scattering, by relatively straightforward modifications such as adding a pump laser or a far field camera.

We have measured diffusion coefficients of Rubidium in Neon, Krypton and Xenon. Reliable values of diffusion coefficients in these gases facilitate setup design and data interpretation in the multimode quantum storage experiments. Moreover we recommend the use of Xenon as a buffer gas in case of Raman interaction and, to the best of our knowledge, we provide the first experimental value of diffusion coefficient in this gas. We believe that this value can also help develop experiments with hyperpolarized Xenon.

ACKNOWLEDGMENTS

We acknowledge generous support from Konrad Banaszek and Rafał Demkowicz-Dobrzański. This work was supported by the Foundation for Polish Science TEAM project, EU European Regional Development Fund and FP7 FET project Q-ESSENCE (Contract No. 248095), National Science Centre grant no. DEC-

2011/03/D/ST2/01941 and by Polish NCBiR under the ERA-NET CHIST-ERA project QUASAR.

[1] L.-M. Duan, M. D. Lukin, J. I. Cirac, and P. Zoller, Nature **414**, 413 (2001).

[2] J. Appel, E. Figueroa, D. Korystov, M. Lobino, and A. Lvovsky, Phys. Rev. Lett. **100**, 093602 (2008).

[3] W. Chalupczak, R. M. Godun, S. Pustelny, and W. Gawlik, Applied Physics Letters **100**, 242401 (2012).

[4] C. F. McCormick, V. Boyer, E. Arimondo, and P. D. Lett, Optics letters **32**, 178 (2007).

[5] M. Fleischhauer, Reviews of Modern Physics **46**, 55 (2005).

[6] A. B. Matsko, O. Kocharovskaya, Y. Rostovtsev, G. R. Welch, A. S. Zibrov, and M. O. Scully, Advances In Atomic, Molecular, and Optical Physics **46**, 191 (2001).

[7] Q. Glorieux, J. B. Clark, A. M. Marino, Z. Zhou, and P. D. Lett, Optics Express **20**, 12350 (2012).

[8] D. Higginbottom, B. Sparkes, M. Rancic, O. Pinel, M. Hosseini, P. Lam, and B. Buchler, Phys. Rev. A **86**, 023801 (2012).

[9] R. Chrapkiewicz and W. Wasilewski, Optics Express **20**, 29540 (2012)
.

[10] O. Firstenberg, M. Shuker, A. Ron, and N. Davidson, Pre-print arXiv:1207.6748 (2012), arXiv:1207.6748
.

[11] M. Shuker, O. Firstenberg, R. Pugatch, A. Ron, and N. Davidson, Physical Review Letters **100** (2008), 10.1103/PhysRevLett.100.223601.

[12] P. K. Vudyasetu, R. M. Camacho, and J. C. Howell, Physical Review Letters **100** (2008), 10.1103/PhysRevLett.100.123901.

[13] M. Shuker, O. Firstenberg, R. Pugatch, A. Ben-Kish, A. Ron, and N. Davidson, Phys. Rev. A **76**, 023813 (2007).

[14] O. Firstenberg, P. London, M. Shuker, A. Ron, and N. Davidson, Nature Phys. **5**, 665 (2009).

[15] W. Franzen, Physical Review **115**, 850 (1959).

[16] F. Franz, Physical Review **139**, A603 (1965).

[17] M. Arditi and T. Carver, Physical Review **136**, A643 (1964).

[18] J. Vanier, J.-F. Simard, and J.-S. Boulanger, Physical Review A **9**, 1031 (1974).

[19] M. Hosseini, B. M. Sparkes, G. Hétet, J. J. Longdell, P. K. Lam, and B. C. Buchler, Nature **461**, 241 (2009).

[20] A. Gozzini, N. Ioli, and F. Strumia, Il Nuovo Cimento B Series 10 **49**, 185 (1967).

[21] P. Bicchi, L. Moi, P. Savino, and B. Zambon, Il Nuovo Cimento B **55**, 1 (1980).

[22] M. A. Bouchiat, The Journal of Chemical Physics **56**, 3703 (1972).

[23] A. Fink, D. Baumer, and E. Brunner, Physical Review A **72**, 053411 (2005).

[24] R. A. Bernheim, The Journal of Chemical Physics **36**, 135 (1962).

[25] R. J. McNeal, The Journal of Chemical Physics **37**, 2726 (1962).

[26] I. Lowe and S. Gade, Physical Review **156**, 817 (1967).

[27] A. Hogervorst, Physica **51**, 59 (1971).